Structure of Restacked MoS_2 and WS_2 Elucidated by Electron Crystallography

Joy Heising and Mercouri G. Kanatzidis*

Contribution from the Department of Chemistry and Center for Fundamental Materials Research, Michigan State University, East Lansing, Michigan 48824

Received August 24, 1998

Abstract: There has been a lot of confusion about the nature of restacked MoS_2 and WS_2. The structure has been proposed to be trigonal TiS_2 type with octahedral M^{4+} and called 1T-MoS_2. The presence of a distortion in the metal plane that gives rise to a superstructure has been suggested. We have performed electron crystallographic studies on small (submicron) single crystal domains of restacked WS_2 and MoS_2 to solve their superstructure. We find that what initially seems to be a trigonal crystal is actually a "triplet" of three individual orthorhombic crystals. Using two-dimensional *hk*0 data from films for both "triple" and "single" crystals we calculated corresponding Patterson projections, which reveal a severe distortion in the Mo/W plane, forming infinite zigzag chains. The projection of the structure suggests M−M distances of 2.92 and 2.74 Å for MoS_2 and WS_2, respectively. Least-squares refinement from the single-crystal data gives $R_1 = 13.3\%$ for WS_2 and $R_1 = 15.3\%$ for MoS_2. Therefore, we submit that restacked MoS_2 and WS_2 are not 1T form but rather WTe_2 type.

Introduction

Due to a unique combination of valuable structural, electronic, and optical properties, the layered dichalcogenides have been studied and used for a litany of practical applications.[1−3] One of the most versatile members of this class of compounds is MoS_2. Found in nature in its 2H form as the mineral molybdenite,[4] its inexpensiveness and availability have permitted its use as a solid lubricant,[1] a catalyst for hydrodesulfurization,[2] a host for intercalcation chemistry, and an electrode material for solid-state batteries.[3]

Many layered transition metal chalcogenides can be treated with *n*-butyllithium to form a reduced species in which lithium occupies the space between the layers.[5] (This ability to undergo reduction and accept lithium is one important reason these materials have been investigated for solid-state batteries.) The redox properties of these reduced dichalcogenides vary from one compound to the next, but some have the remarkable ability to form suspensions in water, much like clays. The chemistry of $LiMoS_2$ (and $LiWS_2$) in water is particularly fascinating because, after undergoing a redox reaction with water to form H_2(g) and LiOH, the layers are "blown apart" into colloidally dispersed single layers, and can remain separated from one another in water for days. The material can be "restacked" by filtration, precipitation, centrifugation, or evaporation. Due to this remarkable ability, many guest species have been encapsulated between the layers.[6−8]

There has been a lot of confusion about the nature of restacked MoS_2 and WS_2. The presence of a distortion in the metal plane which gives rise to a superstructure has been suggested. The reduction of the 2H form appears to induce a structural transformation from trigonal prismatic coordination about the metal to octahedral coordination.[9] The structure has been proposed to be trigonal TiS_2 type[10] with octahedral M^{4+} and called 1T-MoS_2. Originally, 1T-MoS_2 was synthesized by the oxidation of $K_x(H_2O)_yMoS_2$ instead of the exfoliation/restacking method, but the products of both synthetic methods exhibit metallic conductivity and an exothermic transition around 90−100 °C which suggests that they are identical.[11] The layered dichalcogenides are prone to a wide variety of structural distortions caused by charge density waves (CDWs), resulting in significant changes in the properties of the materials.[12] The source of confusion is that several superlattices have been reported for 1T-MoS_2 (Figure 1). EXAFS (extended X-ray absorption fine structure) analyses have indicated M−M associations, but are not able to provide a structural model. X-ray and electron diffraction studies of the restacked MoS_2 (and WS_2) have indicated a $2a \times 2a$ superstructure in the *ab* plane.[13−15] A

(1) Fleischauer, P. D. *Thin Solid Films* **1987**, *154*, 309.
(2) (a) Harris, S.; Chianelli, R. R. *J. Catal.* **1984**, *86*, 400. (b) Brenner, J.; Marshall, C. L.; Ellis, L.; Tomczyk, N.; Heising, J.; Kanatzidis, M. G. *Chem. Mater.* **1998**, *5*, 1244.
(3) Julien, C.; Saikh, S. I.; Nazri, G. A. *Mater. Sci. Eng.* **1992**, *B15*, 73.
(4) Dickinson, R. G.; Pauling, L. *J. Am. Chem. Soc.* **1923**, *45*, 1466.
(5) Murphy, D. W.; DiSalvo, F. J.; Hull, G. W., Jr.; Waszczak, J. V. *Inorg. Chem.* **1976**, *15*, 17.
(6) (a) Divigalpitiya, W. M. R.; Frindt, R. F.; Morrison, S. R. *Science* **1989**, *246*, 369. (b) Divigalpitiya, W. M. R.; Frindt, R. F.; Morrison, S. R. *J. Mater. Res.* **1991**, *6*, 1103. (c) Gee, M. A.; Frindt, R. F.; Morrison, S. R. *Mater. Res. Bull.* **1986**, *21*, 543.
(7) (a) Bissessur, R.; Heising, J.; Hirpo, W.; Kanatzidis, M. G. *Chem. Mater.* **1996**, *8*, 318. (b) Wang, L.; Schindler, J. L.; Thomas, J. A.; Kannewurf, C. R.; Kanatzidis, M. G. *Chem. Mater.* **1995**, *7*, 1753. (c) Kanatzidis, M. G.; Bissessur, R.; DeGroot, D. C.; Schindler, J. L.; Kannewurf, C. R. *Chem. Mater.* **1993**, *5*, 595.
(8) (a) Lemmon, J. P.; Lerner, M. M. *Chem. Mater.* **1994**, *6*, 207. (b) Dungey, K. E.; Curtis, M. D.; Penner-Hahn, J. E. *J. Catalysis* **1998**, *175*, 129.
(9) Py, M. A.; Haering, R. R. *Can. J. Phys.* **1983**, *61*, 76.
(10) Chianelli, R. R.; Scanlon, J. C.; Thompson, A. H. *Mater. Res. Bull.* **1975**, *10*, 1379.
(11) Wypych, F.; Schöllhorn, R. *J. Chem. Soc., Chem. Commun.* **1992**, 1386.
(12) (a) Wilson, J. A.; DiSalvo, F. J.; Mahajan, S. *Adv. Phys.* **1975**, *24*, 117. (b) Wilson, J. A.; DiSalvo, F. J.; Mahajan, S. *Phys. Rev. Lett.* **1974**, *32*, 882.
(13) Yang, D.; Sandovals, S. J.; Divigalpitiya, W. M. R.; Irwin, J. C.; Frindt, R. F. *Phys. Rev. B.* **1991**, *43*, 12053.

10.1021/ja983043c CCC: $18.00
Published on Web 01/14/1999

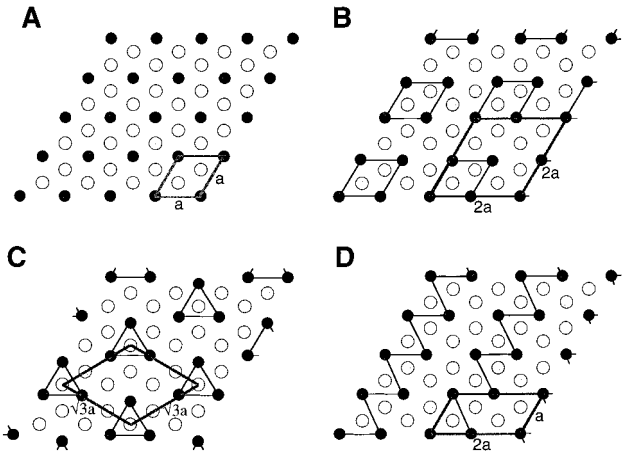

Figure 1. Schematic illustrating the proposed superstructures of restacked/1T-MoS_2. The superstructures derive from bonding associations of metal atoms: **(**A**)** an ideal undistorted lattice, **(**B**)** a tetramerization, **(**C**)** a trimerization, and **(**D**)** a zigzag chain formation. Dark circles represent Mo and gray circles S.

tetramerization model was proposed based on the X-ray diffraction studies.[13] The electron diffraction studies on restacked WS_2, however, found that the hexagonal symmetry was preserved, but the proposed tetramerization model is incompatible with this finding.[14] To add to the confusion, another electron diffraction study on $LiMoS_2$ found the same $2a \times 2a$ superstructure, but the authors attributed it to lithium ordering between the layers.[16] Later, an STM study of the surface layer of restacked MoS_2 suggested a $2a \times a$ superstructure caused by the formation of zigzag chains.[17] The original 1T-MoS_2, however, is reported to exhibit a $\sqrt{3}\cdot a \times \sqrt{3}\cdot a$ superstructure, which would be best described by a trimerization model.[18] In an effort to clarify the structure, we have performed 2-dimensio*nal electron crystallographic* studies on restacked WS_2 and MoS_2. This method has enabled us to probe the bulk material, not just the local environments of the atoms or the structure at the surface. Furthermore, it has allowed us not only to directly determine the structure, but to refine it as well.

X-rays are scattered by the electron shells of atoms; electrons, on the other hand, are scattered by the electrostatic potential due to the atomic nuclei and their electron clouds. Despite the different origins of scattering, much of the theory developed for X-ray crystallography can be applied to electron crystallography and thus, in principle, the two techniques provide similar structural information.[19,20] Most experimentalists have avoided electron diffraction as a technique for structure solution, however, because electrons interact more strongly with the sample than X-rays; hence, multiple scattering events (secondary and dynamic scattering) may take place in electron diffraction.[19,20] Because a TEM (transmission electron microscope) is capable of high magnification, it is possible to acquire data for many samples which cannot be investigated by single-crystal X-ray methods.[19,20] Furthermore, the wavelength of an electron (at an accelerating voltage of 120 kV) is 0.0335 Å, as compared to 0.71 Å for Ka Mo radiation, which (theoretically) can lead to higher resolution data. Because the Ewald sphere is much flatter, many reflections can be observed simultaneously for one orientation of the crystal.[19−22]

We have discovered that, despite the presence of Mo/W in our samples, quasikinematical data are acquired, from which a plausible projection of the structure can be obtained and refined.

Experimental Section

$LiMS_2$ (M = Mo, W) was synthesized by reacting 2H-MS_2 with excess $LiBH_4$ at 300−350 °C for 3 days. Restacked MS_2[6,14] was synthesized by reacting $LiMS_2$ with H_2O, rinsing several times to remove the LiOH generated in the exfoliation process, and depositing the solution on a copper carbon coated grid. The grids were examined at 120 kV on a JEOL 120CX TEM. Suitable crystals were located and their diffraction patterns captured on film. The negatives of the diffraction patterns were scanned into the computer at 600 dpi. The patterns were indexed to an orthorhombic cell with $a = 5.56$ Å and $b = 3.21$ Å, related to the subcell by the relation $\sqrt{3}a_{sub} \times a_{sub}$. The "Gel Plotting" Macro in NIH Image 1.60 was used to extract the integrated intensities (I_{hk0}) from the patterns.[23] Data from 83 cm camera length were used. Accurate cell parameters *a* and *b* were determined from powder diffraction data with a Rigaku-Denki/RW400F2 (Rotaflex) rotating anode powder diffractometer.

The data were converted into *hkl* file format for use in SHELXTL programs.[24] The two-dimensional Patterson maps were calculated from the data by eq 1:

$$P(u, v) = \frac{2}{A}\sum_h \sum_k |\Phi(hk)|^2 \cos 2\pi (hu + kv) \qquad (1)$$

where *P* corresponds to electron density overlap in the structure (i.e. the Patterson function), *A* is the unit cell area, and $|\Phi(hk)| = \sqrt{I_{hk}}$.[10] Least-squares refinement of the structure in SHELXTL (version 5) was carried out after the coefficients for the electron scattering factors were obtained by fitting the sin θ/λ curves with the program Curve Expert.[25]

Results and Discussion

Structure Solution. Because restacked MoS_2 and WS_2 are layered compounds with platelike morphology, they exhibit preferred orientation that causes the *ab* plane to be perpendicular to the electron beam, and the diffraction patterns consistently contained only *hk*0 data. Our initial efforts to locate a suitable crystal resulted in pictures similar to Figure 2. The patterns suggested a $2a \times 2a$ superstructure.[14] Upon consideration, however, we recognized that the exfoliation/flocculation process, involved in the synthesis of restacked MoS_2 and WS_2, would result in turbostratic materials, or at least materials susceptible to stacking faults, and that this could result in pronounced twinning phenomena. We then targeted extremely thin crystals in our investigations and found that, in fact, restacked WS_2 and MoS_2 have a $2a \times a$ superstructure (Figure 3), which is consistent with the results of the STM studies of restacked

(14) Tsai, H. L.; Heising, J.; Schindler, J. L.; Kannewurf, C. R.; Kanatzidis, M. G. *Chem. Mater*., **1997**, *9*, 879.
(15) Yang, D.; Frindt, R. F. *J. Phys. Chem. Solids* **1996**, *57*, 1113.
(16) Chrissafis, K.; Zamani, M.; Kambas, K.; Stoemenos, J.; Economou, N. A.; Samaras, I.; Julien, C. *Mater. Sci. Eng*. **1989**, *B3*, 145.
(17) Qin, X. R.; Yang, D.; Frindt, R. F.; Irwin, J. C. *Ultramicroscopy* **1992**, *42*−*44*, 630.
(18) Wypych, F.; Weber, Th.; Prins, R. *Chem. Mater*. **1998**, *10*, 723.
(19) Vainshtein, B. K. *Structure Analysis by Electron Diffraction*; Pergamon Press, MacMillan Co.: New York, 1964.
(20) Dorset, D. L. *Structural Electron Crystallography*; Plenum Press: New York, 1995.
(21) Stout, G. H.; Jensen, L. H. *X-ray Structure Determination: A Practical Guide*, 2nd ed.; John Wiley & Sons: New York, 1989.
(22) Ladd, M. F. C.; Palmer, R. A. *Structure Determination by X-ray Crystallography*, (3rd ed.; Plenum Press: New York, 1994.
(23) Analysis of integrated intensities was performed on a Macintosh Performa 6214CD computer with use of the public domain NIH Image 1.60 program (developed at the U.S. National Institutes of Health and available on the Internet at http://7/2/98/rsb.info.nih.gov/nih∼image/) with the "Gel Plotting Macros" plug-in.
(24) Sheldrick, G. M. SHELXTL Version 5; Bruker Analytical X-ray Instruments, Inc.: Madison, WI.
(25) Hyams, D. CurveExpert Version 1.34, 1995−1997; Portions copyright 1993, Microsoft Corporation: Seattle, WA.

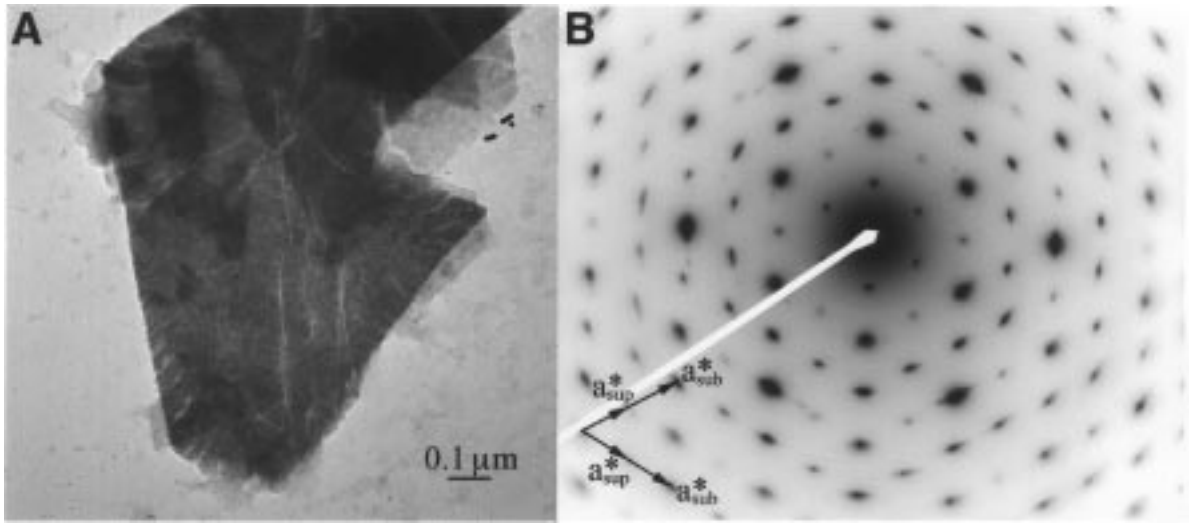

Figure 2. (A) Bright field image and **(**B**)** selected area electron diffraction pattern from a "triple" WS_2 crystal, giving rise to an apparent $2a \times 2a$ hexagonal superstructure.

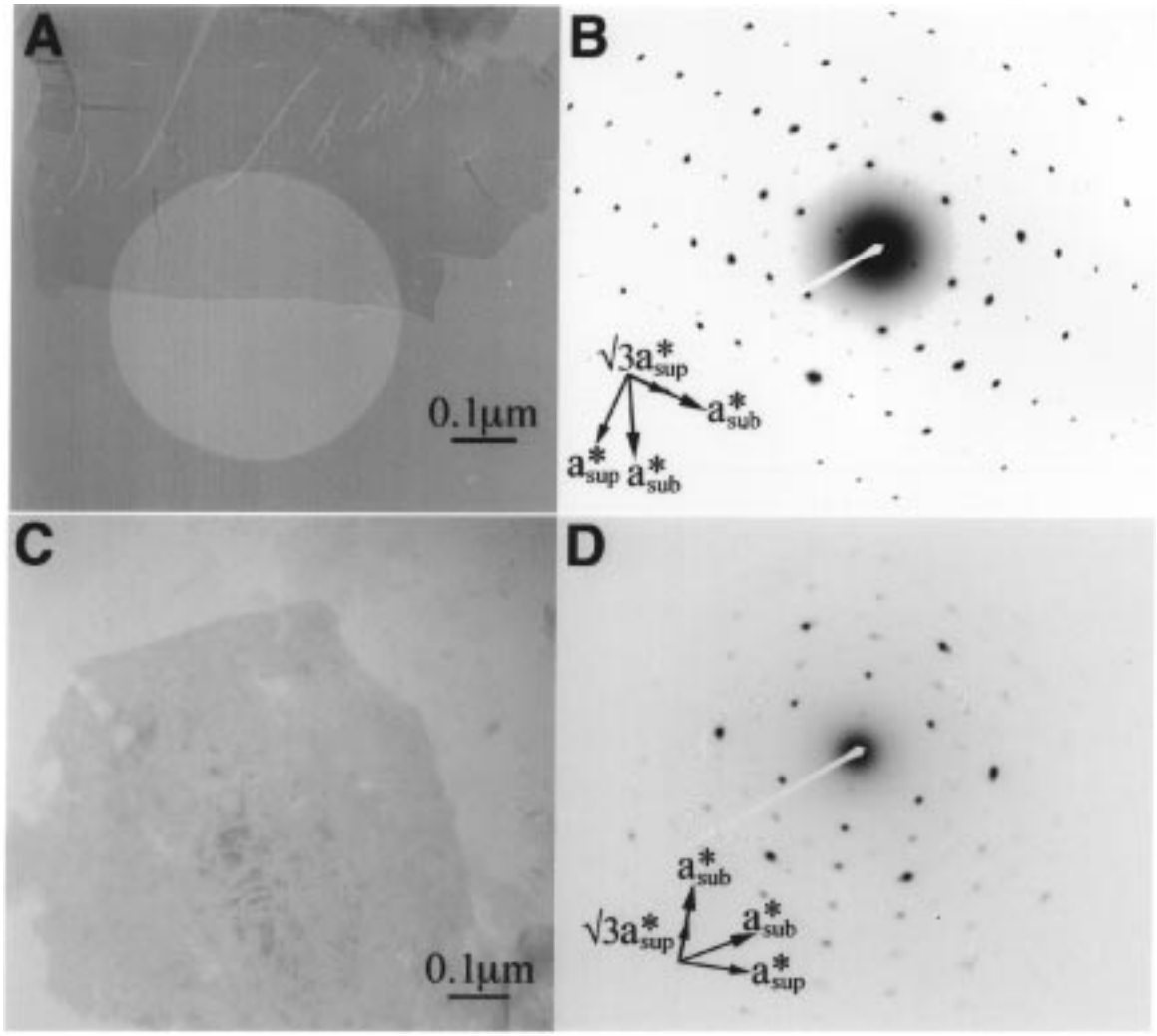

Figure 3. (A) Bright field image and **(**B**)** selected area electron diffraction pattern from a "single" WS_2 crystal, giving rise to a $2a \times a$ or $\sqrt{3}{\cdot}a \times a$ superstructure. **(**C**)** Bright field image and **(**D**)** selected area electron diffraction pattern for MoS_2, giving rise to a $2a \times a$ or a $\sqrt{3}{\cdot}a \times a$ superstructure.

MoS_2.[17] This $2a \times a$ superstructure can actually be more simply described by an orthorhombic $\sqrt{3}{\cdot}a \times a$ cell (Figure 4a). The $2a \times 2a$ superstructure is in fact a "triplet" of three $\sqrt{3}{\cdot}a$ x a crystals rotated by 120° relative to each other. This causes their diffraction spots to be aligned with respect to the sublattice reflections but not the superlattice reflections (Figure 4b). Accordingly, the patterns were indexed to the orthorhombic cell and Patterson maps generated from the data.

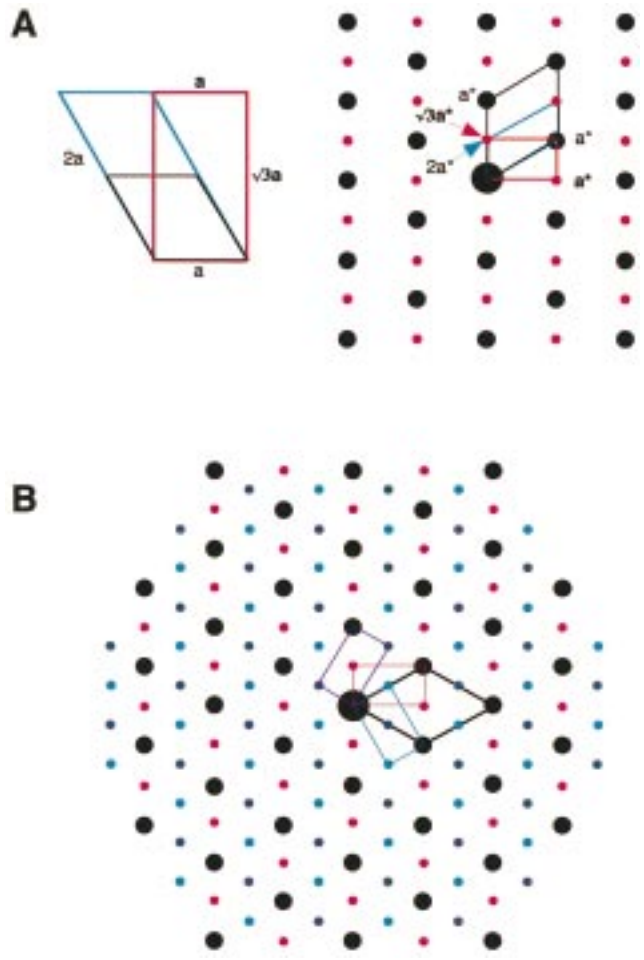

Figure 4. (A) Relationship between a $2a \times a$ and a $\sqrt{3}\cdot a \times a$ lattice. (B) Illustration of how three $\sqrt{3}\cdot a \times a$ patterns can be overlapped to form a $2a \times 2a$ pattern. Note that only the sublattice reflections overlap.

The Patterson maps calculated from the data shown in Figures 2 and 3 clearly indicate a substantial deviation in the metal atom position from the ideal position in the 1T-TiS_2 structure type, which gives rise to a short M−M distance (Figure 5). In an ideal 1T structure the electron density overlap at the center of the Patterson map, which is indicative of the M−M vector in the structure, is circular. In restacked MoS_2 this peak is elongated along the $\sqrt{3}\cdot a$ axis, forming an oval. In restacked WS_2 the distortion is more pronounced, as the M−M vector has split into two resolvable peaks which correspond to two different M−M vectors. In both restacked MoS_2 and WS_2 the other peaks in the Patterson maps, which contain information about the M−S vectors, are also elongated because there are two nonequivalent metal atom positions. This translation of the metal atom along the $\sqrt{3}\cdot a$ axis can only be explained by the formation of zigzag chains. This kind of distortion has been observed in WTe_2, another layered dichalcogenide with (distorted) octahedral coordination about the metal atom.[26]

Least-squares refinement of the structure in SHELXTL (version 5)[24] against a WTe_2 type model gives an R_1 value of 24.6% for the "triple" crystal of WS_2, 13.3% for the "single" crystal of WS_2, and 15.3% for MoS_2 (Table 1). The structure is noncentrosymmetric, belonging to plane group pg (#4). These last two *R* values, although somewhat high by single-crystal X-ray diffraction standards, are very reasonable for refinement involving electron diffraction data.[19,20] This is due to the susceptibility of the electron diffraction data to perturbation by multiple scattering events, as mentioned previously.

This zigzag distortion resembles the structure of WTe_2 and represents a significant departure from the ideal structure, TiS_2 (Figure 6).[26] Distortion of layered octahedral ML_2 d^2 systems to form zigzag chains due to a charge density wave has been predicted by Rovira and Whangbo.[27] This kind of distortion gives rise to changes in the band structure of the material which are consistent with the properties we have observed.[28]

Atomic coordinates and isotropic displacement parameters are given in Table 2. The "single" crystal of WS_2 gives a W−W distance of 2.74 Å, and the MoS_2 data give a Mo−Mo distance of 2.92 Å. The M−M distances have been measured by EXAFS to be 2.74 and 2.8 Å for WS_2 and MoS_2, respectively.[29] Shorter M−M distances than those observed by EXAFS might be explained by displacement of the metal atom along the *c* axis; this displacement is actually observed in WTe_2. Longer M−M distances than those observed by EXAFS may be an artifact of dynamic scattering: we have observed by simulation that the M−M distances appear to increase with increasing thickness.[30] Despite these difficulties, electron crystallography is a more powerful tool for the structure elucidation of these compounds than EXAFS. The latter probes only the local structure, while electron diffraction provides a direct structure determination.

Recently, STM studies on the original 1T-MoS_2, prepared by the oxidation of $K_x(H_2O)_yMoS_2$ with I_2, indicated that it has a $\sqrt{3}\cdot a \times \sqrt{3}\cdot a$ superstructure,[18] as proposed in the original publication reporting the material.[11] It is becoming clear that restacked MoS_2 is not the same as 1T-MoS_2. Other studies have indicated that restacked MoS_2, previously believed to be neutral because of its ability to encapsulate neutral species, has some residual negative charge.[31] The charge balancing species could be Li^+, H^+, or H_3O^+. This residual negative charge apparently stabilizes the structure of restacked MoS_2. STM studies of $K_x(H_2O)_yMoS_2$ suggest that it has the same superstructure as restacked MoS_2.[32]

Dynamic Scattering. As mentioned previously, dynamic scattering is one factor that interferes with structure refinement from electron diffraction data. It has inhibited the widespread use of electron diffraction data for structure determination, particularly in samples containing heavy elements. Although including the effects of dynamic scattering in the refinement should improve the results, it is nonessential for determination of the structure of these materials. This suggests that the use of electron diffraction for structure determination of inorganic materials may not be as unrealistic as previously supposed. Historically, correction for this phenomenon has been attempted in more than one way.[19,20,33−38] The two-beam approximation

(26) (a) Brown, B. E. *Acta Crystallogr*. **1966**, *20*, 268. (b) Mar, A.; Jobic, S.; Ibers, J. A. *J. Am. Chem. Soc.* **1992**, *114*, 8963.

(27) (a) Rovira, C.; Whangbo, M.-H. *Inorg. Chem*. **1993**, *32*, 4094. (b) Whangbo, M.-H.; Canadell, E. *J. Am. Chem. Soc.* **1992**, *114*, 9587.

(28) Bissessur, R.; Kanatzidis, M. G.; Schindler, J. L.; Kannewurf, C. R. *J. Chem. Soc., Chem. Commun*. **1993**, 1582.

(29) (a) Joensen, P.; Crozier, E. D.; Alberding, N.; Frindt, R. F. *J. Phys. C.: Solid State Phys*. **1987**, *20*, 4043. (b) Prouzet, E.; Heising, J.; Kanatzidis, M. G. Unpublished results.

(30) CERIUS^2 Version 3.5 HRTEM module; Molecular Simulations, Inc.: San Diego, CA.

(31) Heising, J.; Bonhomme, F.; Kanatzidis, M. G. *J. Solid State. Chem*. **1998**, in press.

(32) Wypych, F.; Weber, Th.; Prins, R. *Surf. Sci*. **1997**, *380*, L474.

(33) Cowley, J. M.; Moodie, A. F. *Acta Crystallogr*. **1957**, *10*, 609.

(34) Cowley, J. M. *Diffraction Physics*; Elsevier: New York, 1975.

(35) Pinsker, Z. G.; Dvoryankina, G. G. *Kristallografiya* **1958**, *3*, 438.

(36) Spence, J. C. H. *Acta Crystallogr*. **1998**, *A54*, 7.

(37) Sinkler, W.; Marks, L. D.; Edwards, D. D.; Mason, T. O.; Poeppelmeier, K. R.; Hu, Z.; Jorgensen, J. D. *J. Solid State Chem*. **1998**, *136*, 145.

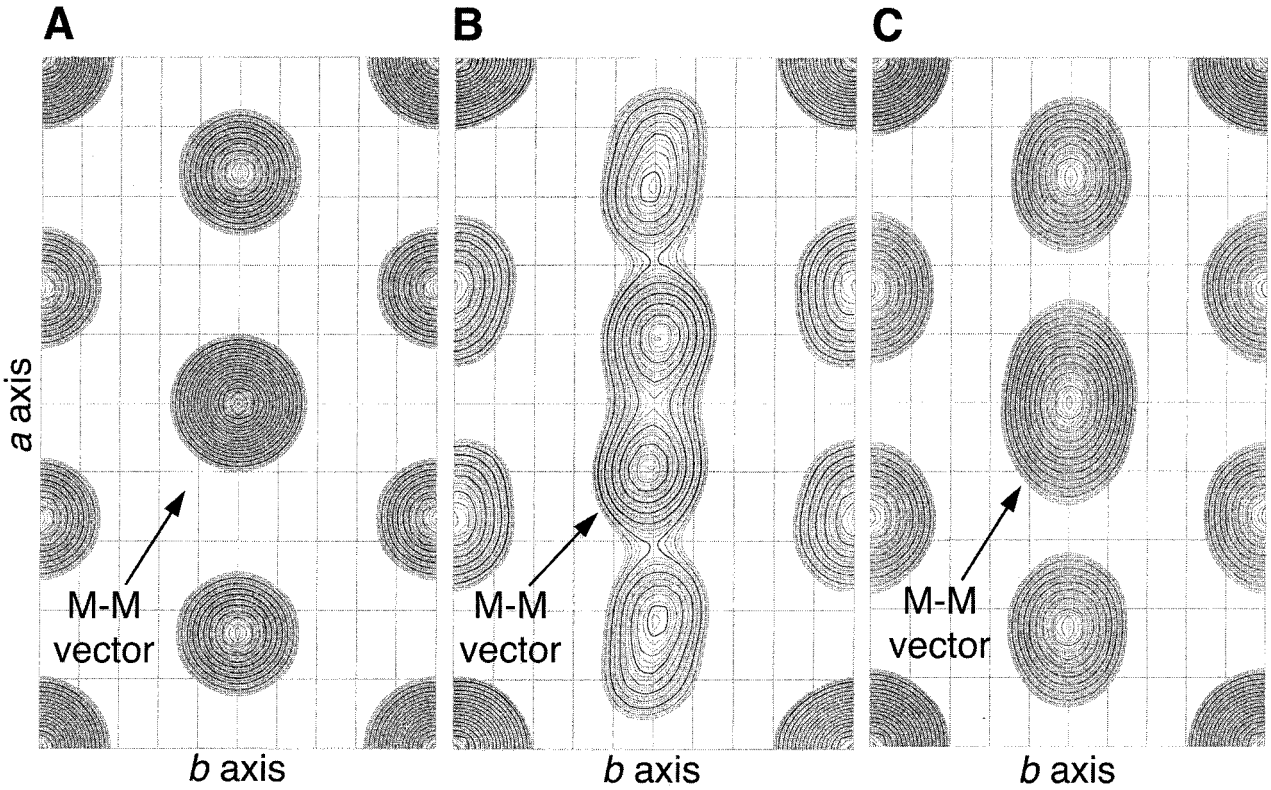

Figure 5. Two-dimensional Patterson projections along the *c* axis: **(**A) ideal 1T-MS_2 (computed from simulated data), (B) restacked WS_2 (computed from experimental data), and **(**C) restacked MoS_2 (computed from experimental data).

Table 1. Crystal Data and Structure Refinement

title	"single" WS_2	"triple" WS_2	MoS_2
empirical formula	WS_2	WS_2	MoS_2
formula weight	248.00	248.00	160.00
temperature	293 K	293 K	293 K
wavelength	0.0335 Å	0.0335 Å	0.0335 Å
crystal system	rectangular	rectangular	rectangular
plane group	pg (#4)	pg (#4)	pg (#4)
unit cell dimensions	$a = 5.56$ Å $b = 3.21$ Å $\gamma = 90°$	$a = 5.56$ Å $b = 3.21$ Å $\gamma = 90°$	$a = 5.47$ Å $b = 3.16$ Å $\gamma = 90°$
area (Å^2)	17.85	17.85	17.29
Z	2	2	2
Φ (000)	46	46	40
2θ range for data collection	0.36 to 2.52°	0.36 to 4.20°	0.36 to 2.78°
data resolution	0.09 to 0.66 sin θ/λ	0.09 to 1.1 sin θ/λ	0.09 to 0.73 sin θ/λ
index ranges	$-7 \le h \le 7, 3 \le k \le 3$	$-12 \le h \le 10, -5 \le k \le 5$	$-7 \le h \le 5, -3 \le k \le 3$
no. of reflections collected	78	173	73
no. of independent reflections	43 [R(int) = 0.1556]	99 [R(int) = 0.0870]	46 [R(int) = 0.2120]
refinement method	full-matrix l.s. on Φ^2	full-matrix l.s. on Φ^2	full-matrix l.s. on Φ^2
data/restraints/parameters	43/0/5	99/0/7	46/0/7
goodness-of-fit on Φ^2	1.305	1.301	1.267
R indices (all data)[a]	$R_1 = 0.1328$	$R_1 = 0.2456$	$R_1 = 0.1525$

[a] $R_1 = \sum(||\Phi_o| - K|\Phi_c||)/\sum|\Phi_o|$.

treats the data as if the intensities of the reflections are composed of scattering from the main beam and from one diffracted beam.[19] In electron diffraction, however, one rarely finds the two-beam approximation to be valid due to the extremely large radius of the Ewald sphere, so alternate approximations, most notably the *n*-beam approximation, have been developed.[20,33,34] The *n*-beam approximation permits the calculation of the dynamic contribution to each reflection from multiple beams. Although more accurate, it is significantly more complicated than the two-beam approximation. Some researchers have combined HRTEM (high-resolution TEM) images with the electron diffraction data to obtain phase information and then used direct methods.[37] Others have combined least-squares refinement with a multislice calculation.[38]

As part of an effort to include a correction for dynamic scattering, the models which resulted from kinematic refinement in SHELX programs were constructed by using the molecular

(38) (a) Zandbergen, H. W.; Andersen, S. J.; Jansen, J. *Science* **1997**, *277*, 1221. (b) Jansen, J.; Tang, D.; Zandbergen, H. W.; Schenk, H. *Acta Crystallogr.* **1998**, *A54*, 91.

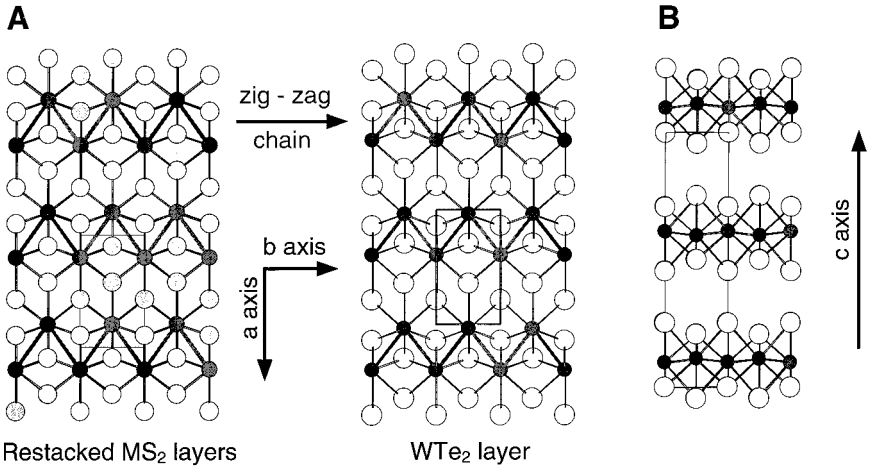

Figure 6. (A) Two-dimensional projection of a restacked MS_2 layer (M = Mo, W) and one WTe_2 layer. (B) View of WTe_2 parallel to the *c* axis. Dark circles are M, gray circles are S, open circles are Te.

Table 2. Atomic Coordinates ($\times 10^4$) and Equivalent Isotropic Displacement Parameters ($A^2 \times 10^3$)

	x	*y*	*U*(eq)[a]	occ
		"single" WS_2		
W(1)	−2021	0	2	1
S(1)	4290	0	8	1
S(2)	950	0	8	1
		MoS_2		
Mo(1)	−2251	0	9	1
S(1)	4240	0	38	1
S(2)	925	0	54	1

[a] *U*(eq) is defined as one-third of the trace of the orthogonalized U_{ij} tensor.

modeling program CERIUS2.[30] This program contains a HR-TEM module that employs the multislice *n*-beam approximation to simulate high-resolution images. Structure factor information for varying thicknesses was extracted from the program and R_1 values were calculated for the simulated data as compared to the experimental data (eq 2):

$$R_1 = \frac{\sum_{hk} ||\Phi_o| - K|\Phi_c||}{\sum_{hk} \Phi_o} \qquad (2)$$

It was observed that increasing thickness appears to "blur" the M−M distance; hence, simulated data for a range of M−M distances were also generated and again R_1 values were calculated. Unfortunately the simulations did not result in significant improvements over kinematic least-squares refinement: the best R_1 value calculated for the "single" WS_2 data set was only ~1.5% lower than the value from the kinematic refinement, and for the MoS_2 data set even the lowest R_1 values were higher than the value from the kinematic refinement. This lack of improvement suggests that there could be other sources of perturbation of the data besides dynamic scattering. For example, the dynamic range of the intensities in the diffraction patterns may exceed the limitations of the electron microscope film and/or the flatbed scanner. This "homogenization" of the intensities would resemble the effects of dynamic scattering, but *n*-beam simulations would not be an appropriate way to compensate for these effects.[39]

Conclusions

In summary, the structure of restacked WS_2 has been determined from electron diffraction data. The 2-D Patterson projection indicates unequivocally that the metal atoms are distorting to form zigzag chains with a short W−W distance of 2.74 Å and a short Mo−Mo distance of 2.92 Å. These distortions are in agreement with earlier theoretical predictions for layered octahedral ML_2 d^2 systems.[27] The results are consistent with those from EXAFS studies, and they are more informative because they provide direct structural information. Structure refinement has been conducted to $R_1 = 13.3\%$ for WS_2 and $R_1 = 15.3\%$ for MoS_2. We conclude that restacked MoS_2 and WS_2 are not 1T-TiS_2 type, but rather WTe_2 type, and that quasi-kinematical electron diffraction data are sufficient for meaningful structure elucidation.

Acknowledgment. Financial Support from the National Science Foundation CHE 96-33798 (Chemistry Research Group) is gratefully acknowledged. This work made use of the TEM facilities at the Center for Electron Optics at Michigan State University. We thank Dr. J. Heckman for fruitful discussion.

JA983043C

(39) The intensities of the *(±020), (±3±10),* and *(±300)* reflections (8 total, 5 unique) were increased by 30%. Least-squares refinement in SHELXTL against corrected and uncorrected data sets revealed no differences in positional parameters and only minor changes in thermal parameters; the net result was a virtually identical solution with slightly lower R_{int} ($\Delta_{max} = 0.5\%$), R_1 ($\Delta_{max} = 1.6\%$), and wR_2 ($\Delta_{max} = 8\%$) values.